ACS APPLIED MATERIALS & INTERFACES

Research Article

Cite This: ACS Appl. Mater. Interfaces 2018, 10, 44511−44517

www.acsami.org

Manganese Vanadium Oxide−N-Doped Reduced Graphene Oxide Composites as Oxygen Reduction and Oxygen Evolution Electrocatalysts

Xiaolin Xing,[†] Rongji Liu,[*,†,‡] Kecheng Cao,[∥] Ute Kaiser,[§,∥] Guangjin Zhang,[‡] and Carsten Streb[*,†,§]

[†]Ulm University, Institute of Inorganic Chemistry I, Albert-Einstein-Allee 11, 89081 Ulm, Germany

[‡]Key Laboratory of Green Process and Engineering, Institute of Process Engineering, Chinese Academy of Sciences, 100190, Beijing, China

[§]Helmholtz-Institute Ulm for Electrochemical Energy Conversion, Helmholtzstrasse 11, 89081 Ulm, Germany

[∥]Central Facility of Electron Microscopy for Materials Science, Ulm University, 89081 Ulm, Germany

Supporting Information

ABSTRACT: The oxygen evolution reaction (OER) and oxygen reduction reaction (ORR) are key catalytic processes for sustainable energy technologies, such as water electrolysis or fuel cells. Here, a novel metal oxide−nanostructured carbon composite is reported, which acts as OER and ORR electrocatalyst under technologically relevant conditions. A facile synthetic process allows the deposition of a molecular manganese vanadium oxide precursor, $[Mn_4V_4O_{17}(OAc)_3]^{3-}$, on reduced graphene oxide. Simultaneously, the precursor is converted into insoluble nanostructured solid-state Mn−V-oxide catalysts. Control of the synthetic conditions allows tuning of the electrocatalytic properties of the composites, leading to excellent and stable electrochemical reactivity. The electrocatalytic ORR and OER activity was evaluated in alkaline aqueous electrolyte and showed performance comparable with commercial Pt/C electrocatalysts. The study thus demonstrates how polyoxometalate precursors based on earth-abundant elements can be deposited on nanostructured carbon to give high-performance OER/ORR catalysts for alkaline water electrolysis. A new class of composite catalysts can in future be accessed by a facile fabrication route.

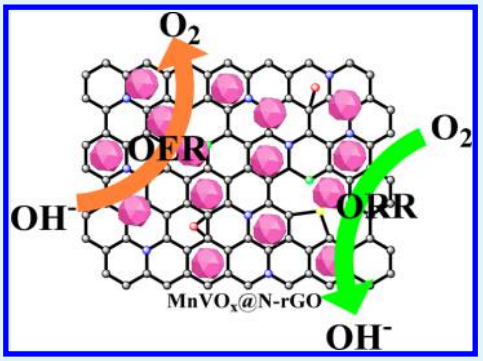

KEYWORDS: *reduced graphene oxide, polyoxometalate, oxygen reduction reaction, oxygen evolution reaction, bifunctional electrocatalysts*

1. INTRODUCTION

The development of sustainable energy technologies, such as water electrolysis,[1] metal−air batteries,[2,3] and fuel cells[4] relies on earth abundant catalysts, which efficiently catalyze the oxygen reduction reaction (ORR) and the oxygen evolution reaction (OER).[5−8] To this end, 3d transition metal oxides are ideal catalyst candidates, as they combine earth abundant elements with high catalytic performance, facile synthesis, and high stability under harsh chemical conditions. In particular, manganese oxides have attracted significant interest as ORR and OER catalysts because of their low cost, earth-abundance, low toxicity, good cycling stability, and catalytic activity.[9−14] Currently, the development of this materials class is hampered by their large band gaps, leading to low intrinsic electrical conductivity. In addition, material stability and catalytic performance are key properties, which require further optimization. To this end, new mixed-metal oxides were designed to improve the ORR/OER performance, leading to 3d metal-based catalysts such as $MnCo_2O_4$,[15,16] $MnFe_2O_4$,[17] or $CoFe_2O_4$.[18] Often, these materials were synthesized by thermal decomposition of two separate compounds, which give little control over the final material composition, morphology, and chemical structure. Thus, facile and efficient fabrication routes for mixed-metal oxide catalysts are still a major challenge in materials chemistry.

One promising precursor class are molecular metal oxides—so-called polyoxometalates (POMs). POMs are a family of early transition metal (TM)-oxo clusters widely used as electrocatalysts for challenging reactions including the ORR and OER.[19,20] Recently, POM-derived porous nanocarbon composites, containing metal carbides, nitrides, sulfides, or oxides, have attracted increasing attention in the field of electrochemical energy conversion and storage.[20−22] Nanostructured mixed metal oxides are easily accessible by thermal decomposition when using mixed-metal-based POMs as precursors because the metal ratio in the POM precursors is

Received: September 26, 2018
Accepted: December 3, 2018
Published: December 3, 2018

DOI: 10.1021/acsami.8b16578
ACS Appl. Mater. Interfaces 2018, 10, 44511−44517

predefined.[20] We have demonstrated the feasibility of this approach recently and developed bottom-up approaches to deposit manganese vanadium oxides[23] on conductive substrates, for example, nanostructured carbons.[24]

Over recent years, reduced graphene oxide (rGO) has attracted significant interest as conductive catalyst support as it combines excellent conductivity, high surface area and outstanding chemical stability. Further, rGO can be modified to feature reactive surface groups (e.g., alcohols, amines), which are suitable for anchoring metal oxide catalysts, leading to a number of electrocatalytic composites.[25−29] Also, N-doped nanocarbon materials, especially carbon nanotubes and graphene, have shown surprising catalytic activity for the ORR.[30,31] However, the combination of catalytically active, stable metal oxide, and electrically conductive, nanostructured carbonaceous support is still a major challenge for modern materials chemistry and facile, scalable syntheses are urgently required to enable further progress in the field.

Here, we report the facile bottom-up fabrication of ORR/OER electrocatalyst composites formed by controlled deposition of molecular manganese vanadium oxide precursors on functionalized nitrogen-doped rGO substrates. The method presented combines easy, scalable synthesis with chemical tunability on the molecular level, so that in the current example, we can access a composite material based only on earth-abundant components. The resulting $MnVO_x$@N-rGO composites demonstrate high ORR and OER activity and combine long-term stability with reactivity under technologically important conditions, so that based on this synthetic concept, a wide range of related composites becomes accessible. Tuning of elemental composition, structure and morphology of the composite can be used to tune catalytic performance and stability.

2. EXPERIMENTAL SECTION

2.1. Instrumentation. *2.1.1. High-Resolution Transmission Electron Microscopy (HRTEM).* HRTEM measurements were performed with an image-side aberration corrected FEI TITAN 80−300 under an accelerating voltage of 80 kV.

2.1.2. Powder X-ray Diffraction (pXRD). Powder X-ray diffraction studies were performed on a BRUKER D8 Advance XRD unit using Cu Kα (λ = 1.54 Å).

2.1.3. X-ray Photoelectron Spectroscopy (XPS). XPS analysis was performed on ESCALAB250 Thermo Electron Corporation equipment with an Al Ka X-ray source (1486.6 eV). The X-ray source was run at a reduced power of 150 W, and the pressure in the analysis chamber was maintained at 10−11 Pa or lower.

2.1.4. General Remarks. All chemicals were purchased from Sigma-Aldrich, ABCR or ACROS and were of reagent grade. The chemicals were used without further purification unless stated otherwise. $\{Mn_4V_4\}$ was prepared according to reference.[14] For comparison, TEM images of the sonicated $\{Mn_4V_4\}$ were recorded and show dense aggregate structures formed by nanoparticles with diameters between ∼10 and 40 nm (Figure S1a and b).

2.2. Synthesis of the Composite Materials. GO was dispersed in anhydrous acetonitrile (ACN). The concentration of the final GO/ACN suspension was ∼1 mg/mL.

For the N-rGO synthesis, 2.21 mL of 35% aqueous NH_4OH solution was added to 30 mL of GO/ACN suspension. The reaction was stirred at 80 °C for 12 h. Then, the reaction mixture was transferred to a 120 mL autoclave for hydrothermal reaction at 180 °C for 6 h, and the N-rGO was obtained. The resulting product was collected by centrifugation, washed with ethanol and dried.

To prepare the $MnVO_x$@N-rGO composites, first, 5 mL of 0.018 mM $\{Mn_4V_4\}$[14] ACN solution was added into 30 mL of GO/ACN suspension (∼1 mg/mL), followed by the addition of 2.21 mL of NH_4OH (35% aqueous solution). The reaction was stirred at 80 °C with stirring for 12 h. Then, the reaction mixture from the first step was transferred to a 120 mL autoclave for hydrothermal reaction at 180 °C for 6 h. The resulting product was collected by centrifugation and washed with ethanol, then dried at 60 °C for 12 h. The collected solid was further heat-treated at 440 °C for 4 h (giving **1−440**) or 900 °C for 1 h (giving **1−900**).

2.3. Electrochemical Studies. All electrochemical measurements were performed on an electrochemical workstation (CHI 730 E, CH Instruments, Inc. U.S.A) at room temperature using a standard three-electrode electrochemical cell. A Pt wire and an Ag/AgCl electrode in 3 M aqueous KCl were used as the counter and reference electrodes, respectively. All potentials in this study are given versus reversible hydrogen electrode (RHE). E(RHE) = E(Ag/AgCl) + 0.210 + 0.059pH, here 0.210 V is the standard potential for Ag/AgCl electrode at 25 °C. A glassy carbon rotating disk electrode (RDE) with 4.0 mm diameter and a rotating Pt ring-glassy carbon disk electrode (RRDE, disk diameter 4.0 mm; Pt ring inner diameter 6.0 mm, outer diameter 8.0 mm) were used as working electrode for evaluating the ORR and OER performance.

For all electrochemical measurements, the modified electrodes were used as working electrodes and prepared by the following method: 4 mg of the as-prepared catalyst, 20 μL of Nafion solution (5% w/w in water and 1-propanol, Nafion D-520, Germany) and 2 mL of ethanol were mixed by at least of 1 h of sonication to form a homogeneous ink. The catalyst ink (18.8 μL) was pipetted onto the surface of glassy carbon working electrode and air-dried. Unless stated otherwise, the catalyst loading was 0.3 mg cm^{-2}. For comparison, a commercial Pt/C (20 wt % Pt on Vulcan carbon black fromPremetek Co.) was deposited on the working electrode with the same procedure and tested for ORR and OER under identical conditions.

For the ORR measurements, the modified RDE was used as the working electrode and the experiment was performed in an O_2-saturated solution using linear sweep voltammetry (LSV) at a scan rate of 10 mV s^{-1} with varying rotating speed from 400 to 1600 rpm.

To study the activity and selectivity of the catalyst for oxygen reduction, the modified RRDE was used as the working electrode and the LSV was recorded at a scan rate of 10 mV s^{-1} at 1600 rpm, and the ring potential was kept constantly at 1.45 V vs RHE.

3. RESULTS AND DISCUSSION

3.1. Composite Synthesis. Deposition of Mn−V-oxides on N-rGO was achieved as illustrated in Scheme 1. The Mn−V-oxide cluster $[Mn_4V_4O_{17}(OAc)_3]^{3-}$ ($\{Mn_4V_4\}$)[14] was used as a molecular precursor, and was mixed with graphene oxide (GO) in acetonitrile/aqueous ammonia. The solution was heated to 80 °C for 12 h, which led to the oxidation of $\{Mn_4V_4\}$ and the growth of $MnVO_x$ nanoparticles on GO sheets. Then, hydrothermal treatment at 180 °C for 6 h enabled the crystallization of $MnVO_x$ and also the reduction and nitrogen-doping of GO, leading to N-doped reduced

Scheme 1. Schematic Illustration of the $MnVO_x$@N-rGO Composite Synthesis

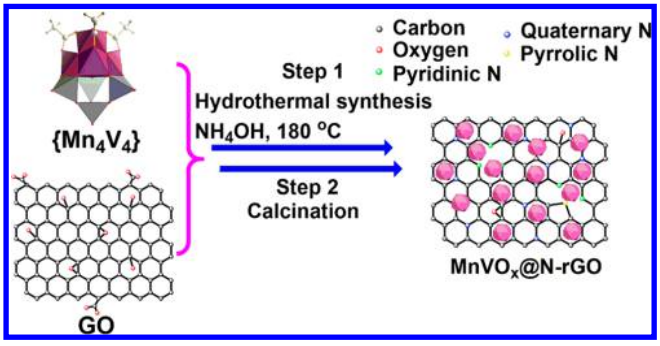

DOI: 10.1021/acsami.8b16578
ACS Appl. Mater. Interfaces 2018, 10, 44511−44517

graphene oxide (N-rGO).[32] The solid product was separated, dried and thermally treated under Argon atmosphere at 440 °C (named **1−440**) or 900 °C (named **1−900**), leading to the formation of crystalline manganese vanadium oxide phases stably linked to the N-rGO.

3.2. Characterization. Initial structural characterization of the samples was carried out using powder X-ray diffraction (pXRD). Figure 1 shows the pXRD patterns of as-synthesized

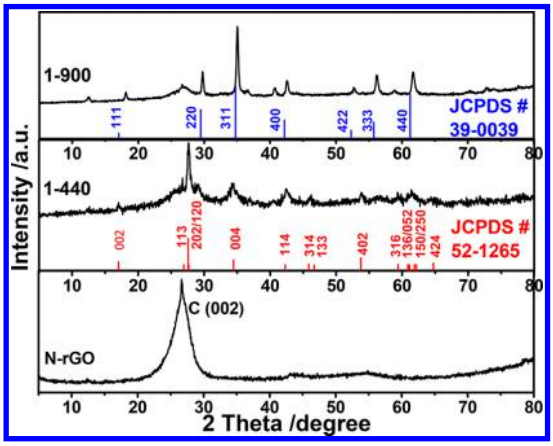

Figure 1. Powder X-ray diffractograms of N-rGO, **1−440**, and **1−900**.

N-rGO and the $MnVO_x$@N-rGO composites. The broad peak in the range between 22 and 28° is assigned to noncrystalline, defective N-rGO.[33] The metal oxides present in the composites calcined at 440 and 900 °C can be indexed to $Mn_2V_2O_7$ (JCPDS 52-1265 in **1−440**) and $Mn_{1.5}V_{1.5}O_4$ (JCPDS 3-90039 in **1−900**), respectively (Figure 1). The peaks of the composites showed a slight shift toward higher diffraction angles as compared to the pristine oxides, indicating a reduced interplanar spacing, which could be due to the calcination process.

The structure and morphology of the composites was studied by high-resolution transmission electron microscopy (HRTEM). For **1−900**, Figure 2a shows that spherical $Mn_{1.5}V_{1.5}O_4$ nanoparticles (average size 7−10 nm) are homogeneously distributed on wrinkled N-rGO sheets. The manganese vanadium oxide particles feature lattice fringes with spacings of 0.210, 0.258, and 0.295 nm (Figures 2 and S1c and d), which are in agreement with the (400), (311), and (220) lattice planes of $Mn_{1.5}V_{1.5}O_4$. For **1−440**, HRTEM indicates crystalline manganese oxide particles with fringe spacings of 0.197 nm, 0.214 and 0.250 nm (Figures 2 and S1e and f), which are in line with the (314), (114), and (004) lattice planes of $Mn_2V_2O_7$. Inductively coupled plasma optical emission spectroscopy (ICP-OES) also gave a Mn/V atomic ratio of ∼1.09 for **1−440** and ∼1.10 for **1−900**, which are consistent with the structural analysis. Note that all $MnVO_x$ particles observed by TEM are anchored to the N-rGO matrix, confirming the successful, stable linkage between metal oxide and the N-rGO substrate.

X-ray photoelectron spectroscopy (XPS) was performed to investigate the composition and oxidation states of the composites. XPS spectra of both composites (Figure S2) confirm the presence of Mn, V, C, and N. As shown in Figure 3a and c, both **1−440** and **1−900** feature manganese centers in oxidation state Mn^{2+}, Mn^{3+}, and Mn^{4+}. This is in line with the previously reported data for $Mn_2V_2O_7$ (JCPDS 52-1265) and

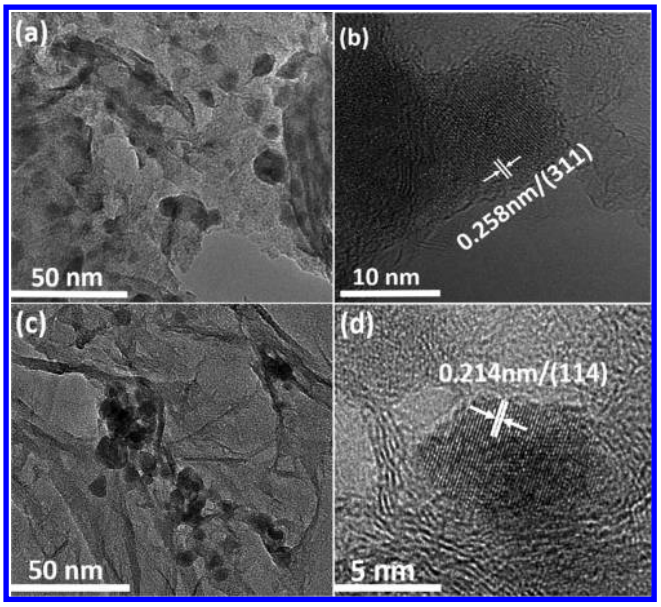

Figure 2. HRTEM images of (a, b) **1−900** and (c, d) **1−440**, showing the lattice fringes of crystalline manganese vanadium oxide particles deposited on N-rGO.

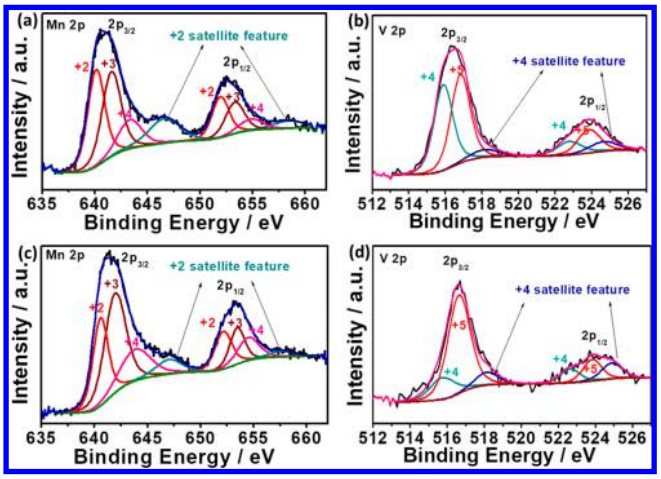

Figure 3. Manganese and vanadium XPS spectra for **1−440** (a, b) and **1−900** (c, d).

$Mn_{1.5}V_{1.5}O_4$ (JCPDS 39-0039) and highlights the mixed-oxidation-states of both manganese oxides. In detail, for **1−440**, the Mn $2p_{3/2}$ can be deconvoluted into three peaks (640.1, 641.6, and 643.3 eV), originating from the +2, +3, and +4 oxidation states of Mn in the surface of the composite, respectively.[34−36] Similar spectral features are also observed for **1−900**. The Mn 3s spectra (Figure S2a and d) for both **1−440** and **1−900** show Mn 3s exchange splitting (a well-known effect in transition metals which is a sensitive probe of the local magnetic moment) of 6.20 and 6.03 eV further confirm the coexistence of Mn species in oxidation states Mn^{2+}, Mn^{3+}, and Mn^{4+}.[34−36] Notably, mixed-oxidation state manganese compounds have previously been proposed as highly active ORR and OER electrocatalysts,[36−38] For both **1−440** and **1−900** (Figure 3b and d), the vanadium XPS spectra can be deconvoluted into contributions from V^{4+} and V^{5+}, indicating that vanadium is also present in mixed oxidation states.[39]

Analysis of the N 1s spectra (see Figure S2b and e) for both composites indicates the presence of pyridinic N, pyrrolic N,

DOI: 10.1021/acsami.8b16578
ACS Appl. Mater. Interfaces 2018, 10, 44511−44517

quaternary N, and oxidized N, respectively. Note that previous reports highlighted the importance of pyridinic and quaternary nitrogen as active sites for the ORR, so that in future, tuning of the composites could allow the further optimization of the ORR reactivity.[40,41] Closer inspection shows that **1−900** features significantly less pyrrolic N but more quaternary N compared with **1−440**, indicating that the calcination procedure can be used to tune the chemical nitrogen environment within the composites. Further, in both composites, the C 1s spectra (see Figure S2c and f) indicate the presence of C−C/C═C, C−N, and C−O species and are in line with previous reports on related compounds,[42] supporting the presence of N-doped rGO as support material. For **1−900**, we note a decreased intensity of C−O and disappearance of the C═O signal (compared to **1−440**), indicating that most of the oxidized C functionalities can be removed by calcination, leading to rGO with improved electronic conductivity, which is in line with recent literature reports.[43]

3.3. ORR Activity. The electrocatalytic performance of the $MnVO_x$@N-rGO composites was evaluated by ORR polarization curves using RDE measurements in O_2-saturated 0.1 M aqueous KOH solution. Figure 4a and c shows the

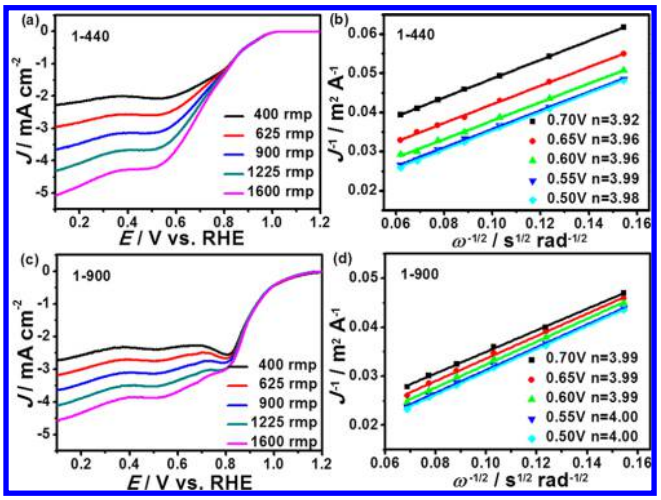

Figure 4. Linear sweep voltammograms (LSV) recorded by RDE in O_2 saturated 0.1 M aqueous KOH solution at different rotation rates for **1−440** (a) and **1−900** (c). Panels b and d show Koutecky−Levich plots of J^{-1} versus $\omega^{-1/2}$ for the corresponding **1−440** and **1−900** at different electrode potentials, respectively.

corresponding LSVs. For both **1−440** and **1−900**, the current densities increase with increasing rotation rates, which is due to the faster mass transport on the electrode surface. The limiting current densities observed (at 1600 rpm) were 5.3 (**1−440**) and 4.5 mA cm^{-2} (**1−900**), respectively. The onset potential (E_{onset}) and half-wave potential ($E_{1/2}$) of 1−900 (E_{onset} = 1.14 V, $E_{1/2}$ = 0.80 V) are significantly more positive than the corresponding values for **1−440** (E_{onset} = 0.98 V, $E_{1/2}$ = 0.66 V) and the nonmodified N-rGO reference (E_{onset} = 0.800 V, $E_{1/2}$ = 0.39 V, Figure S3a), indicating the superior catalytic activity of the composite containing $Mn_{1.5}V_{1.5}O_4$ as catalyst (also see Tables 1 and S1 for more details). For comparison, we also performed the ORR for native $\{Mn_4V_4\}$ deposited on a glassy carbon electrode. However, for this system, we observed very poor catalytic activity, and more negative onset potentials and significantly lower current

Table 1. ORR and OER Performance of the Composites Studied

composite	E_{ORR} at J = −3 mA cm^{-2} (V vs RHE)	E_{OER} at J = 10 mA cm^{-2} (V vs RHE)	$\Delta E_{OER-ORR}$ (V vs RHE)
1−440	0.66	1.67	1.01
1−900	0.80	1.65	0.85
Pt/C	0.81	>2.00	>1.2

density were noted (Figure S4a). This emphasizes the importance of proper electrical "wiring" of the metal oxide and nanostructured carbon for improved charge transfer and resulting catalytic reactivity.[44]

Next, we determined the electron transfer number n via the Koutecky−Levich equation.[45] This allows us to rationalize whether the catalysts operate by a two-step two-electron or one-step four-electron O_2 reduction.[46] For nonmodified N-rGO and the native $\{Mn_4V_4\}$ (Figures S3b and S4b), we observed electron transfer numbers of ∼2−3 at all potentials studied, indicating that the oxygen reduction proceeded by two consecutive two-electron processes and the formation of hydrogen peroxide (HO_2^-) as intermediate. In contrast, both **1−440** and **1−900** composites show electron transfer numbers of ∼4 at potentials between 0.5 and 0.7 V (Figure 4b and d), suggesting an efficient four-electron transfer pathway in ORR catalysis with no peroxide formation. This is critical for the long-term stability of the catalyst, as peroxides are often degrading the catalytic device.[47] Thus, catalyst stability was explored by performing chronoamperometry (CA) for **1−900** (E = 0.7 V vs. RHE) in 0.1 M aqueous KOH with RDE as working electrode. As shown in Figure S5a, no significant changes in current density were observed over a period of 4 h, indicating the high durability of the composite during ORR. Further, similar CVs of **1−900** are observed before and after CA (Figure S5b), illustrating that no major electrochemical changes are observed during the long-term CA test.

Next, we used RRDE measurements to record LSV data to compare the electrocatalytic ORR performance of the composites with a commercial Pt/C electrocatalyst. Figure 5a shows the ring and disk currents recorded by RRDE at 1600 rpm in 0.1 M aqueous KOH electrolyte for **1−440**, **1−900**, and commercial Pt/C as a reference. The terminal disk currents produced by the composites were close to that of Pt/C, showing similar performance. Small ring currents indicate

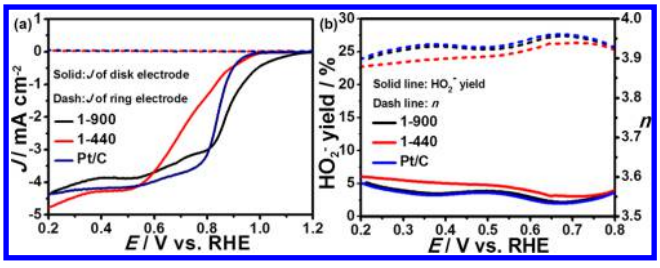

Figure 5. (a) Rotating ring−disk electrode voltammograms of **1−440** and **1−900** compared with commercial Pt/C. Conditions: O_2-saturated 0.1 M aqueous KOH at 1600 rpm. The disk potential was scanned at 10 mV/s and the ring potential was kept constant at 1.45 V vs RHE. (b) Hydroperoxide formation (as percentage of total oxygen reduction products) and electron transfer number n for **1−900**, **1−440**, and Pt/C at various potentials based on the corresponding RRDE data in panel a. Catalyst loading amount was 0.3 mg cm^{-2} for all samples.

DOI: 10.1021/acsami.8b16578
ACS Appl. Mater. Interfaces 2018, 10, 44511−44517

that only small amounts (<10%) of the nondesired hydroperoxides are formed, providing further evidence for the efficient four-electron O_2 reduction pathway by the composites. **1−900** showed the highest electrocatalytic ORR activity with a onset potential of 1.13 V vs RHE, while **1−440** and commercial Pt/C had more negative onset potentials of 0.99 and 0.96 V vs RHE, respectively. Note that the calculated electron transfer number n for all three materials was ∼3.9, which suggests a four-electron reduction.[48] Figure S6 shows the corresponding Tafel plots where Tafel slopes of 130.9 (**1−900**), 66.6(**1−440**), and 85.4 mV dec^{-1} (Pt/C) were determined.

In sum, these analyses confirm the excellent electrocatalytic activity and stability of the composites and highlight how facile materials design based on molecular earth-abundant materials can be used to develop novel, technologically relevant electrocatalyst composites.

3.4. OER Activity. Next, we analyzed the OER activity of the composites. To this end, **1−440** and **1−900** were deposited on carbon fiber paper (CFP), and LVS analyses were performed in 0.1 M aqueous KOH (Figure 6a). The

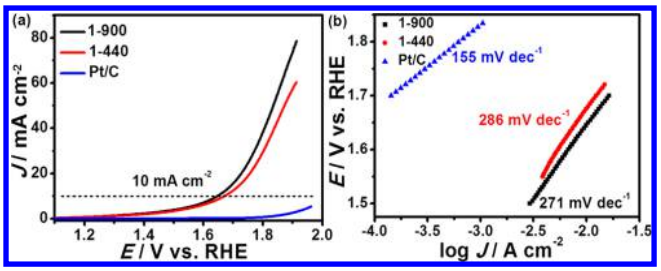

Figure 6. (a) Linear scan voltammograms (LSV) of **1−900**, **1−440**, and Pt/C in 0.1 M KOH. The LSV was measured in O_2-saturated solution with a scan rate of 10 mV s^{-1} and catalyst loading of 1 mg cm^{-2} on carbon fiber paper; (b) the corresponding Tafel plots derived from LSV in panel a.

oxygen evolution potential at a current density of J = 10 mA cm^{-2} was used as established standard for comparison of catalytic activity.[48] Both composites show good catalytic activity with OER potentials of 1.67 V (**1−440**) and 1.65 V (**1−900**), which are comparable to recently published high-performance catalysts (see Table S1). As shown in Figure S7a, LSVs of **1−900** were recorded before and after electrochemical cycling. We observed a positive potential shift of ∼25 mV (at J = 10 mA cm^2) after 1500 cycles. This minor change highlights the high stability of the composite during OER. Furthermore, CVs of **1−900** before and after potential cycles (Figure S7b) are virtually identical and further support the promising long-term stability of the composite. While the Tafel slopes were 271 and 286 mV for **1−900** and **1−400**, respectively, highlighting that further materials design is required to optimize OER performance of the composites (see Figure 6b). For comparison, the Pt/C reference was also examined and showed low activity with significantly larger overpotential (but lower Tafel slope) than the composites. As reference, we compared the OER performance of native N-rGO and native $\{Mn_4V_4\}$, both deposited on glassy carbon electrodes. For both references, we observed lower OER activity, thus providing further evidence for the superior catalytic performance of the composite (see Figure S8). To gain further insight into the different electrocatalytic activities of **1−440** and **1−900**, we performed electrochemical impedance spectrometry (EIS)of the composites, see SI, Figure S9. Lower impedance was observed for **1−900** compared with **1−440**, so that the improved electronic conductivity of **1−900** could be one reason for the higher electrocatalytic performance of this composite.

Examination of the potential difference ($\Delta E_{OER\text{-}ORR}$)[49] between the OER potential (at J = of 10 mA cm^{-2}) and the ORR potential (at J = −3 mA cm^{-2}) provides an evaluation of the overall oxygen electrode activity, and small $\Delta E_{OER\text{-}ORR}$ values are desired for optimum reversible oxygen electrode performance. The comparison shows that **1−900** features the lowest potential difference (0.85 V) of the OER/ORR catalysts examined (Table 1). The values observed for **1−900** are comparable to noble-metal-based bifunctional OER/ORR catalyst models, such as Ir/C (0.92 V),[50] Ru/C (1.01 V),[35] and also many nonprecious metal-based bifunctional OER/ORR catalysts.[48] For comprehensive comparison, see Table S1.

4. CONCLUSION

In summary, we report a facile synthetic route leading to highly active ORR/OER electrocatalysts with performance comparable to noble-metal-based systems. Deposition of a molecular manganese vanadium oxide precursor on graphene oxide and thermal annealing gives access to nanoparticulate Mn−V-oxides stably linked to high surface-area nitrogen-doped reduced graphene oxide. Two different crystalline Mn−V oxide phases can be accessed, both of which show promising ORR reactivity and high long-term stability even under harsh electrocatalytic conditions. Both catalysts also feature promising OER reactivity and show virtually identical overpotentials, highlighting that the reactivity limitation is most likely not related to the structural features of the catalyst.

Future work will explore in details the interfacial electron transfer within the compounds to establish limitations and means for materials optimization. This could allow us to explore the use of these systems under technological conditions with a focus on water electrolysis and fuel cells.

■ ASSOCIATED CONTENT

Supporting Information

The Supporting Information is available free of charge on the ACS Publications website at DOI: 10.1021/acsami.8b16578.

For materials, instrumentation, characterization, synthetic, and electrocatalytic details (PDF)

■ AUTHOR INFORMATION

Corresponding Authors

*E-mail: carsten.streb@uni-ulm.de.

*E-mail: rongji.liu@uni-ulm.de.

ORCID

Carsten Streb: 0000-0002-5846-1905

Author Contributions

X.X. and R.L. contributed equally to this work. X.X. performed materials synthesis and characterization. X.X. and R.L. performed the electrochemical and electrocatalytic tests. K.C. and U.K. performed TEM analyses. All authors cowrote the manuscript. All authors have given approval to the final version of the manuscript.

Notes

The authors declare no competing financial interest.

DOI: 10.1021/acsami.8b16578
ACS Appl. Mater. Interfaces 2018, 10, 44511−44517

■ ACKNOWLEDGMENTS

Ulm University, the Deutsche Forschungsgemeinschaft (STR1164/4, STR1164/12, TRR234 "CataLight" Projects B3 and C4), Helmholtz-Institute Ulm (HIU), the National Natural Science Foundation of China (No. 91545125), and the Chinese Academy of Sciences President's International Fellowship Initiative (2018VMA0041) are acknowledged for financial support. X.X. acknowledges the Chinese Scholarship Council (CSC) for a doctoral fellowship. R.L. acknowledges the Alexander-von-Humboldt-Foundation for a postdoctoral fellowship. This work contributes to the research performed in CELEST (Center for Electrochemical Energy Storage Ulm-Karlsruhe).

■ REFERENCES

(1) Rossmeisl, J.; Qu, Z. W.; Zhu, H.; Kroes, G. J.; Nørskov, J. K. Electrolysis of Water on Oxide Surfaces. *J. Electroanal. Chem.* **2007**, *607*, 83−89.

(2) Armand, M.; Tarascon, J.-M. Building Better Batteries. *Nature* **2008**, *451*, 652−657.

(3) Christensen, J.; Albertus, P.; Sanchez-Carrera, R. S.; Lohmann, T.; Kozinsky, B.; Liedtke, R.; Ahmed, J.; Kojic, A. A Critical Review of Li−Air Batteries. *J. Electrochem. Soc.* **2012**, *159*, R1−R30.

(4) Gewirth, A. A.; Thorum, M. S. Electroreduction of Dioxygen for Fuel-Cell Applications: Materials and Challenges. *Inorg. Chem.* **2010**, *49*, 3557−3566.

(5) Ghosh, S.; Kar, P.; Bhandary, N.; Basu, S.; Sardar, S.; Maiyalagan, T.; Majumdar, D.; Bhattacharya, S. K.; Bhaumik, A.; Lemmens, P.; Pal, S. K. Microwave-Assisted Synthesis of Porous Mn_2O_3 Nanoballs as Bifunctional Electrocatalyst for Oxygen Reduction and Evolution Reaction. *Catal. Sci. Technol.* **2016**, *6*, 1417−1429.

(6) Gorlin, Y.; Lassalle-Kaiser, B.; Benck, J. D.; Gul, S.; Webb, S. M.; Yachandra, V. K.; Yano, J.; Jaramillo, T. F. In Situ X-Ray Absorption Spectroscopy Investigation of a Bifunctional Manganese Oxide Catalyst with High Activity for Electrochemical Water Oxidation and Oxygen Reduction. *J. Am. Chem. Soc.* **2013**, *135*, 8525−8534.

(7) Kottakkat, T.; Bron, M. One-Pot Synthesis of Cobalt-Incorporated Nitrogen-Doped Reduced Graphene Oxide as an Oxygen Reduction Reaction Catalyst in Alkaline Medium. *ChemElectroChem* **2014**, *1*, 2163−2171.

(8) Liu, X.; Li, L.; Zhou, W.; Zhou, Y.; Niu, W.; Chen, S. High-Performance Electrocatalysts for Oxygen Reduction Based on Nitrogen-Doped Porous Carbon from Hydrothermal Treatment of Glucose and Dicyandiamide. *ChemElectroChem* **2015**, *2*, 803−810.

(9) Kuo, C.-H.; Mosa, I. M.; Thanneeru, S.; Sharma, V.; Zhang, L.; Biswas, S.; Aindow, M.; Pamir Alpay, S.; Rusling, J. F.; Suib, S. L.; He, J. Facet-Dependent Catalytic Activity of MnO Electrocatalysts for Oxygen Reduction and Oxygen Evolution Reactions. *Chem. Commun.* **2015**, *51*, 5951−5954.

(10) Pickrahn, K. L.; Park, S. W.; Gorlin, Y.; Lee, H. B. R.; Jaramillo, T. F.; Bent, S. F. Active MnO x Electrocatalysts Prepared by Atomic Layer Deposition for Oxygen Evolution and Oxygen Reduction Reactions. *Adv. Energy Mater.* **2012**, *2*, 1269−1277.

(11) Duan, J.; Chen, S.; Dai, S.; Qiao, S. Z. Shape Control of Mn_3O_4 Nanoparticles on Nitrogen-Doped Graphene for Enhanced Oxygen Reduction Activity. *Adv. Funct. Mater.* **2014**, *24*, 2072−2078.

(12) Zhang, T.; Cheng, F.; Du, J.; Hu, Y.; Chen, J. Efficiently Enhancing Oxygen Reduction Electrocatalytic Activity of MnO2 Using Facile Hydrogenation. *Adv. Energy Mater.* **2015**, *5*, 1400654.

(13) Sun, W.; Hsu, A.; Chen, R. Carbon-Supported Tetragonal MnOOH Catalysts for Oxygen Reduction Reaction in Alkaline Media. *J. Power Sources* **2011**, *196*, 627−635.

(14) Schwarz, B.; Forster, J.; Goetz, M. K.; Yücel, D.; Berger, C.; Jacob, T.; Streb, C. Visible-Light-Driven Water Oxidation by a Molecular Manganese Vanadium Oxide Cluster. *Angew. Chem., Int. Ed.* **2016**, *55*, 6329−6333.

(15) Cheng, F.; Shen, J.; Peng, B.; Pan, Y.; Tao, Z.; Chen, J. Rapid Room-Temperature Synthesis of Nanocrystalline Spinels as Oxygen Reduction and Evolution Electrocatalysts. *Nat. Chem.* **2011**, *3*, 79−84.

(16) Chen, D.; Chen, C.; Baiyee, Z. M.; Shao, Z.; Ciucci, F. Nonstoichiometric Oxides as Low-Cost and Highly-Efficient Oxygen Reduction/Evolution Catalysts for Low-Temperature Electrochemical Devices. *Chem. Rev.* **2015**, *115*, 9869−9921.

(17) Zhu, H.; Zhang, S.; Huang, Y.-X.; Wu, L.; Sun, S. Monodisperse $M_xFe_{3-x}O_4$ (M = Fe, Cu, Co, Mn) Nanoparticles and Their Electrocatalysis for Oxygen Reduction Reaction. *Nano Lett.* **2013**, *13*, 2947−2951.

(18) Indra, A.; Menezes, P. W.; Sahraie, N. R.; Bergmann, A.; Das, C.; Tallarida, M.; Schmeißer, D.; Strasser, P.; Driess, M. Unification of Catalytic Water Oxidation and Oxygen Reduction Reactions: Amorphous Beat Crystalline Cobalt Iron Oxides. *J. Am. Chem. Soc.* **2014**, *136*, 17530−17536.

(19) Zhang, S.; Oms, O.; Hao, L.; Liu, R.; Wang, M.; Zhang, Y.; He, H. Y.; Dolbecq, A.; Marrot, J.; Keita, B.; Zhi, L. J.; Mialane, P.; Li, B.; Zhang, G. J. High Oxygen Reduction Reaction Performances of Cathode Materials Combining Polyoxometalates, Coordination Complexes, and Carboneous Supports. *ACS Appl. Mater. Interfaces* **2017**, *9*, 38486−38498.

(20) Chen, C.; Wu, A.; Yan, H.; Xiao, Y.; Tian, C.; Fu, H. Trapping $[PMo_{12}O_{40}]^{3-}$ Clusters into Pre-Synthesized ZIF-67 toward Mo_xCo_xC Particles Confined in Uniform Carbon Polyhedrons for Efficient Overall Water Splitting. *Chem. Sci.* **2018**, *9*, 4746−4755.

(21) Li, J.-S.; Wang, Y.; Liu, C.-H.; Li, S.-L.; Wang, Y.-G.; Dong, L.-Z.; Dai, Z.-H.; Li, Y.-F.; Lan, Y.-Q. Coupled Molybdenum Carbide and Reduced Graphene Oxide Electrocatalysts for Efficient Hydrogen Evolution. *Nat. Commun.* **2016**, *7*, 11204.

(22) Tang, Y. J.; Gao, M. R.; Liu, C. H.; Li, S. L.; Jiang, H. L.; Lan, Y. Q.; Han, M.; Yu, S. H. Porous Molybdenum-Based Hybrid Catalysts for Highly Efficient Hydrogen Evolution. *Angew. Chem., Int. Ed.* **2015**, *54*, 12928−12932.

(23) Ji, Y.; Hu, J.; Biskupek, J.; Kaiser, U.; Song, Y.-F.; Streb, C. Polyoxometalate-Based Bottom-Up Fabrication of Graphene Quantum Dot/Manganese Vanadate Composites as Lithium Ion Battery Anodes. *Chem. - Eur. J.* **2017**, *23*, 16637−16643.

(24) Ji, Y.; Huang, L.; Hu, J.; Streb, C.; Song, Y. Polyoxometalate-Functionalized Nanocarbon Materials for Energy Conversion, Energy Storage and Sensor Systems. *Energy Environ. Sci.* **2015**, *8*, 776−789.

(25) Sun, L.; Zhou, L.; Yang, C.; Yuan, Y. CeO_2 Nanoparticle-Decorated Reduced Graphene Oxide as an Efficient Bifunctional Electrocatalyst for Oxygen Reduction and Evolution Reactions. *Int. J. Hydrogen Energy* **2017**, *42*, 15140−15148.

(26) Liu, K.; Li, J.; Wang, Q.; Wang, X.; Qian, D.; Jiang, J.; Li, J.; Chen, Z. Designed Synthesis of $LaCoO_3$/N-Doped Reduced Graphene Oxide Nanohybrid as an Efficient Bifunctional Electrocatalyst for ORR and OER in Alkaline Medium. *J. Alloys Compd.* **2017**, *725*, 260−269.

(27) Lin, S.; Zhao, X. S.; Li, Y. F.; Liang, C.; Huang, K.; Sheng, Y.; Wang, H.; Ye, C. X.; Xu, X.; Zhou, Y. F.; Fan, D. Y.; Shang, Y. F.; Yang, H. J.; Zhang, R.; Wang, Y. G.; Lei, M. One-Step Synthesis of Ag-Reduced Graphene Oxide Nanocomposites and Their Surface-Enhanced Raman Scattering Activity. *Powder Diffr.* **2014**, *29*, 356−360.

(28) El-Kady, M. F.; Strong, V.; Dubin, S.; Kaner, R. B. Laser Scribing of High-Performance and Flexible Graphene-Based Electrochemical Capacitors. *Science* **2012**, *335*, 1326−1330.

(29) Ghosh, S.; Remita, H.; Kar, P.; Choudhury, S.; Sardar, S.; Beaunier, P.; Roy, P. S.; Bhattacharya, S. K.; Pal, S. K. Facile Synthesis of Pd Nanostructures in Hexagonal Mesophases as a Promising Electrocatalyst for Ethanol Oxidation. *J. Mater. Chem. A* **2015**, *3*, 9517−9527.

(30) Gong, K.; Du, F.; Xia, Z.; Durstock, M.; Dai, L. Nitrogen-Doped Carbon Nanotube Arrays with High Electrocatalytic Activity for Oxygen Reduction. *Science* **2009**, *323*, 760−764.

DOI: 10.1021/acsami.8b16578
ACS Appl. Mater. Interfaces 2018, 10, 44511−44517

(31) Qu, L.; Liu, Y.; Baek, J.-B.; Dai, L. Nitrogen-Doped Graphene as Efficient Metal-Free Electrocatalyst for Oxygen Reduction in Fuel Cells. *ACS Nano* **2010**, *4*, 1321−1326.
(32) Luo, D.; Zhang, G.; Liu, J.; Sun, X. Evaluation Criteria for Reduced Graphene Oxide. *J. Phys. Chem. C* **2011**, *115*, 11327−11335.
(33) Chen, H.; Müller, M. B.; Gilmore, K. J.; Wallace, G. G.; Li, D. Mechanically Strong, Electrically Conductive, and Biocompatible Graphene Paper. *Adv. Mater.* **2008**, *20*, 3557−3561.
(34) Sambandam, B.; Soundharrajan, V.; Song, J.; Kim, S.; Jo, J.; Duong, P. T.; Kim, S.; Mathew, V.; Kim, J. Investigation of Li-Ion Storage Properties of Earth Abundant B-$Mn_2V_2O_7$ prepared Using Facile Green Strategy. *J. Power Sources* **2017**, *350*, 80−86.
(35) Zhao, L.; Lin, S.; Bi, K.; Liang, C.; Du, Y.; Liu, J.; Yang, H.; Fan, D.; Wang, Y.; Lei, M. Manganese Vanadium Oxide Hollow Microspheres: A Novel Electrocatalyst for Oxygen Reduction Reaction. *J. Solid State Electrochem.* **2017**, *21*, 1743−1749.
(36) Stoerzinger, K. A.; Risch, M.; Suntivich, J.; Lü, W. M.; Zhou, J.; Biegalski, M. D.; Christen, H. M.; Ariando; Venkatesan, T.; Yang, S. H. Oxygen Electrocatalysis on (001)-Oriented Manganese Perovskite Films: Mn Valency and Charge Transfer at the Nanoscale. *Energy Environ. Sci.* **2013**, *6*, 1582−1588.
(37) Jin, K.; Park, J.; Lee, J.; Yang, K. D.; Pradhan, G. K.; Sim, U.; Jeong, D.; Jang, H. L.; Park, S.; Kim, D.; Sung, N. E.; Kim, S. H.; Han, S.; Nam, K. T. Hydrated Manganese(II) Phosphate ($Mn_3(PO_4)_2 \cdot 3H_2O$) as a Water Oxidation Catalyst. *J. Am. Chem. Soc.* **2014**, *136*, 7435−7443.
(38) Ryabova, A. S.; Napolskiy, F. S.; Poux, T.; Istomin, S. Y.; Bonnefont, A.; Antipin, D. M.; Baranchikov, A. Y.; Levin, E. E.; Abakumov, A. M.; Kéranguéven, G.; Antipov, E. V.; Tsirlina, G. A.; Savinova, E. R. Rationalizing the Influence of the Mn(IV)/Mn(III) Red-Ox Transition on the Electrocatalytic Activity of Manganese Oxides in the Oxygen Reduction Reaction. *Electrochim. Acta* **2016**, *187*, 161−172.
(39) Silversmit, G.; Depla, D.; Poelman, H.; Marin, G. B.; De Gryse, R. Determination of the V2p XPS Binding Energies for Different Vanadium Oxidation States (V^{5+} to V^{0+}). *J. Electron Spectrosc. Relat. Phenom.* **2004**, *135*, 167−175.
(40) Rao, C. V.; Cabrera, C. R.; Ishikawa, Y. In Search of the Active Site in Nitrogen-Doped Carbon Nanotube Electrodes for the Oxygen Reduction Reaction. *J. Phys. Chem. Lett.* **2010**, *1*, 2622−2627.
(41) Lai, L.; Potts, J. R.; Zhan, D.; Wang, L.; Poh, C. K.; Tang, C.; Gong, H.; Shen, Z.; Lin, J.; Ruoff, R. S. Exploration of the Active Center Structure of Nitrogen-Doped Graphene-Based Catalysts for Oxygen Reduction Reaction. *Energy Environ. Sci.* **2012**, *5*, 7936.
(42) Wang, H.; Maiyalagan, T.; Wang, X. Review on Recent Progress in Nitrogen-Doped Graphene: Synthesis, Characterization, and Its Potential Applications. *ACS Catal.* **2012**, *2*, 781−794.
(43) Liu, R.; Li, S.; Yu, X.; Zhang, G.; Zhang, S.; Yao, J.; Keita, B.; Nadjo, L.; Zhi, L. Facile Synthesis of Au-Nanoparticle/Polyoxometalate/Graphene Tricomponent Nanohybrids: An Enzyme-Free Electrochemical Biosensor for Hydrogen Peroxide. *Small* **2012**, *8*, 1398−1406.
(44) Hu, J.; Ji, Y.; Chen, W.; Streb, C.; Song, Y.-F. Wiring Redox-Active Polyoxometalates to Carbon Nanotubes Using a Sonication-Driven Periodic Functionalization Strategy. *Energy Environ. Sci.* **2016**, *9*, 1095−1101.
(45) Bard, A. J.; Faulkner, L. R. *Electrochemical Methods Fundamentals and Applications*; Wiley, 1944.
(46) Paulus, U. A.; Schmidt, T. J.; Gasteiger, H. A.; Behm, R. J. Oxygen Reduction on a High-Surface Area Pt/Vulcan Carbon Catalyst: A Thin-Film Rotating Ring-Disk Electrode Study. *J. Electroanal. Chem.* **2001**, *495*, 134−145.
(47) Ramaswamy, N.; Hakim, N.; Mukerjee, S. Degradation Mechanism Study of Perfluorinated Proton Exchange Membrane under Fuel Cell Operating Conditions. *Electrochim. Acta* **2008**, *53*, 3279−3295.
(48) Fu, G.; Yan, X.; Chen, Y.; Xu, L.; Sun, D.; Lee, J. M.; Tang, Y. Boosting Bifunctional Oxygen Electrocatalysis with 3D Graphene Aerogel-Supported Ni/MnO Particles. *Adv. Mater.* **2018**, *30*, 1704609.
(49) Cheon, J. Y.; Kim, K.; Sa, Y. J.; Sahgong, S. H.; Hong, Y.; Woo, J.; Yim, S. D.; Jeong, H. Y.; Kim, Y.; Joo, S. H. Graphitic Nanoshell/Mesoporous Carbon Nanohybrids as Highly Efficient and Stable Bifunctional Oxygen Electrocatalysts for Rechargeable Aqueous Na-Air Batteries. *Adv. Energy Mater.* **2016**, *6*, 1501794.
(50) Gorlin, Y.; Jaramillo, T. A Bifunctional Nonprecious Metal Catalyst for Oxygen Reduction and Water Oxidation. *J. Am. Chem. Soc.* **2010**, *132*, 13612−13614.

DOI: 10.1021/acsami.8b16578
ACS Appl. Mater. Interfaces 2018, 10, 44511−44517